CHARACTERIZATION OF SURFACES ON AN ATOMIC SCALE BY FIELD IONIZATION ENERGY SPECTRA

Andrew J. Jason, et al

Alabama University

Prepared for:

Air Force Office of Scientific Research
Advanced Research Projects Agency

1 August 1975

ARPA
No. 2780

CHARACTERIZATION OF SURFACES ON AN ATOMIC SCALE BY FIELD IONIZATION ENERGY SPECTRA

Final Report

Grant AFOSR 74-2726
Program Code 4D10

Andrew J. Jason and Albert C. Parr

Department of Physics
University of Alabama
University, Alabama 35486

SPONSORED BY

ADVANCED RESEARCH PROJECTS AGENCY

ARPA ORDER NO 2780

UNCLASSIFIED

SECURITY CLASSIFICATION OF THIS PAGE (When Data Entered)

REPORT DOCUMENTATION PAGE		READ INSTRUCTIONS BEFORE COMPLETING FORM
1. REPORT NUMBER AFOSR - TR - 75 - 1463	2. GOVT ACCESSION NO.	3. RECIPIENT'S CATALOG NUMBER
4. TITLE (and Subtitle) Characterization of Surfaces on an Atomic Scale by Field Ionization Energy Spectra		5. TYPE OF REPORT & PERIOD COVERED Final 6. PERFORMING ORG. REPORT NUMBER
7. AUTHOR(s) Andrew J. Jason Albert C. Parr		8. CONTRACT OR GRANT NUMBER(s) AFOSR 74-2726
9. PERFORMING ORGANIZATION NAME AND ADDRESS The University of Alabama Department of Physics & Astronomy P. O. Box 1921, University, AL 35486		10. PROGRAM ELEMENT, PROJECT, TASK AREA & WORK UNIT NUMBERS 9761-02 A02780 61102F 681304
11. CONTROLLING OFFICE NAME AND ADDRESS Advanced Research Projects Agency 1400 Wilson Blvd. Arlington, VA 22209		12. REPORT DATE 8-1-75 13. NUMBER OF PAGES 44
14. MONITORING AGENCY NAME & ADDRESS(if different from Controlling Office) AFOSR/NE 1400 Wilson Blvd. Arlington, VA 22209		15. SECURITY CLASS. (of this report) UNCLASSIFIED 15a. DECLASSIFICATION/DOWNGRADING SCHEDULE

16. DISTRIBUTION STATEMENT (of this Report)

Approved for public release; distribution unlimited

17. DISTRIBUTION STATEMENT (of the abstract entered in Block 20, if different from Report)

18. SUPPLEMENTARY NOTES

19. KEY WORDS (Continue on reverse side if necessary and identify by block number)

Field Ionization, Surface Physics, Surface Ion Emission
Field Ionization Energy Spectra, Field Ion Microscopy

20. ABSTRACT (Continue on reverse side if necessary and identify by block number)

Field ionization energy spectra of ions produced at a metallic surface are studied in order to relate the distributions in energy to surface properties. The technique provides information about the mechanical and electronic properties of the surface on the level of single surface atoms. Instrumentation details are discussed and experimental results of the project given. Examples of energy distributions are given and the experimental relationship between distributions and imaging gas properties is discussed.

DD FORM 1 JAN 73 1473 EDITION OF 1 NOV 65 IS OBSOLETE

UNCLASSIFIED

SECURITY CLASSIFICATION OF THIS PAGE (When Data Entered)

CHARACTERIZATION OF SURFACES ON AN ATOMIC SCALE BY FIELD IONIZATION ENERGY DISTRIBUTIONS

by

Andrew J. Jason and Albert C. Parr

Final Report

Grant Number AFOSR 74-2726
Program Code 4D10

Department of Physics and Astronomy
The University of Alabama
University, Alabama 35486

Sponsored by

Advanced Research Projects Agency
ARPA Order No. 2780

TABLE OF CONTENTS

SUMMARY - Final Technical Report, AFOSR 74-2726

Energy spectra of ions formed by field ionization at single atomic surface sites are studied. Information relevant to the configurational and energy structure of the surface are contained in the energy spectra. In particular, the work has applications to the study of surface defects, multi-compositional surfaces and catalysis. The appropriate energy and spatial resolutions are provided by the combination of a 12-inch radius magnetic analyzer with a field-ion microscope as an ion source. The field-ion microscope provides ions imaged to a magnified representation of the surface so that emissions from single atomic sites are resolved. The magnetic analyzer acts as a high resolution differential energy analyzer to determine the energy spectra.

Experiments and theory indicate that features of the energy distributions are related to the band structure of the metal above the Fermi level and other surface properties such as the reflectivity for electron scattering. This is hence a corollary technique to field emission spectrometry which is limited to energies below the Fermi level. Energy distributions are systematically measured as a function of position on the surface and the effects of various imperfections and defects explored. This technique also has implications for study of alloy surfaces. Details of these implications can be found in the original proposal.

The instrumentation has been designed and constructed to accommodate the experiments discussed. The vacuum system achieves pressures on the order of 10^{-9} to 10^{-10} Torr. In addition to the differential analysis capability of the magnetic sector, a high resolution retarding lens system allows for integral energy analysis of the ion beams. The retarding analysis is

particularly useful in determining the absolute energy scale of spectra. The magnetic analyzer is field regulated to provide field stability to better than a part in 10^5. The data acquisition instrumentation includes a pulse counting system, a multiscaler, and a custom designed synchronized voltage sweep system as well as conventional integrating readouts.

The field ion image is optically coupled to an image intensifier with optical gain of up to 10^6. This allows for simultaneous viewing of the field ion image and measurement of the ion energy distribution with unambiguous identification of the region of the surface monitored. The entire source end of the instrument is cryogenically cooled to liquid hydrogen or helium temperatures. Further instrumental details are contained in the Instrumentation section of this report.

Experiments have been performed with hydrogen as the imaging gas and tungsten as the field-ion emitter. The results show the secondary peak structure previously observed. Data acquisition is performed by pulse storage techniques resulting in an enhanced signal to statistical noise ratio. Further data is given demonstrating instrument resolution capabilities when used as a differential analyzer.

A study of the relation between distribution onsets and sample gas ionization potential has been made. A linear relationship between the ionization potential and energy onset of the parent ion in field ionization was substantiated. The results have implications for determining energetics of surface-gas interaction on energy spectra. In addition, this suggests a new technique for measuring appearance potentials of substances that are involatilizable or fragment extensively by conventional techniques.

A further paper has been submitted for publication entitled "Energy Spectra of Organic Molecules in Field Ionization" which further explores the relation between the imaging gas structure and energy spectra. This paper is included as the Appendix.

Field ionization energy analysis promises to be a very useful tool in the study of surfaces. In particular it appears to be a method that can give information about the surface on a microscopic scale.

I. INTRODUCTION

This is the final technical report under grant AFOSR 74-2726, "Characterization of Surfaces on an Atomic Scale by Field Ionization Energy Spectra", begun May 13, 1974. The second section of the report discusses the current theoretical and experimental situation in the literature updating the references in our original proposal.[1] The third section discusses some instrumental aspects of the work while the fourth section details experimental progress.

The project was undertaken to study the energy spectra of ions produced in a high electric field near a surface. This phenomenon, known as field ionization, is utilized in the field-ion microscope[2] to produce a highly magnified representation of a surface and hence, obtain microscopically detailed information on surface structure and processes. In this project, investigation of information inherent in the field-ion microscope is extended and supplemented by additionally exploring the energy spectra of field ions, with particular effort toward resolving events occurring above single surface atoms. Theoretical considerations and preliminary experimental results indicate that field ionization energy spectroscopy is a promising technique for surface studies. We are developing the technique and obtaining results for systems of interest. In particular, it is believed that the results of this study will aid in specifying local atomistic structure of defects and imperfections on the surface of metal crystals.

The grant period of one year has been devoted mainly to development of techniques and refinement of instrumentation. Progress has been made in specifying and obtaining energy distributions from small areas of the surface. The data obtained is under analysis. In addition, work has been completed on measurements relating the onset energies of the spectra to the ionization potential of the imaging gas and these results, constituting two papers, are to be published.

II. CURRENT THEORETICAL AND EXPERIMENTAL SITUATION

We have proposed the energy spectra technique as a means of investigating band structure above the Fermi level in metallic samples[1] and have published results which were thus interpreted.[1,3] Recently Utsumi and Smith[4] have obtained similar results by a retarding technique with an expanded interpretation of the spectra. These results show that the field ionization spectra are detailed and are a function of surface conditions and structure.

Work by Appelbaum[5] lends support to our contention that the details of secondary peaks in the energy distributions are measures of electron scattering by the crystal. Using LEED data and a semi-empirical approach Appelbaum has been able to obtain a good fit to experimental data. In addition to measuring the electron reflection coefficient the energy spectra are found to determine the phase of the reflection coefficient.

Müller and coworkers[6,7] have recently obtained results on the secondary structure which verify our observations. In this work the ionization rate is measured as a function of energy deficit by optical monitoring of a channel plate electron multiplier.

Hanson, Humes, and Inghram[8] and Hanson[9] have investigated the energy distributions of mulecular hydrogen isotopes. In particular, they have found interesting effects due to molecular rotation after ionization. This study is of particular interest to us because it allows distinction between molecular effects and effects due to the surface, thus clarifying the interpretation of results using hydrogen as imaging gas.

III. INSTRUMENTATION: It was felt appropriate to describe the instrumentation unique to this project.

A. General

A 12" radius of curvature, 60 degree magnetic sector mass spectrometer has been constructed for use as a mass analyzer and as an ion energy analyzer. Figure 1 shows the instrument and some of the accompanying electronics. Figure 2 gives a schematic diagram of the instrument. The vacuum system for the instrument is constructed of stainless steel and inconel and is entirely bakeable. The system is pumped statically with ion pumps. A turbomolecular pump is used for rough pumping and to aid in differentially pumping high sample loads. The system routinely achieves pressures of 10^{-9} to 10^{-10} Torr.

The emitter is mounted on moveable gimbals with ruby ball bearings. The gimbals are micrometrically adjustable through a bellows sealed linkage from outside the vacuum system. Figure 3A shows the gimbal mount. The field-ion image is formed on a fluorescent screen attached to the beam defining aperture of the ion lens system. Hole sizes on the order of a size of the image of a single surface atom can be used for this aperture.

B. Ion Optics and Energy Analysis

The ion lens system is shown in Figures 3D through 3G. Figure 3F shows the complete ion lens system and the entrance slit to the mass spectrometer. The entrance slit, adjustable from outside the vacuum, is at the top of Figure 3F. An electric quadrupole doublet lens system, shown in the lower part of Figure 3F astigmatically focuses the circular ion beam onto the entrance slit of the magnetic analyzer or of the retarder lens. Figure 3G shows the ion lens system mounted on the instrument. The retarding energy

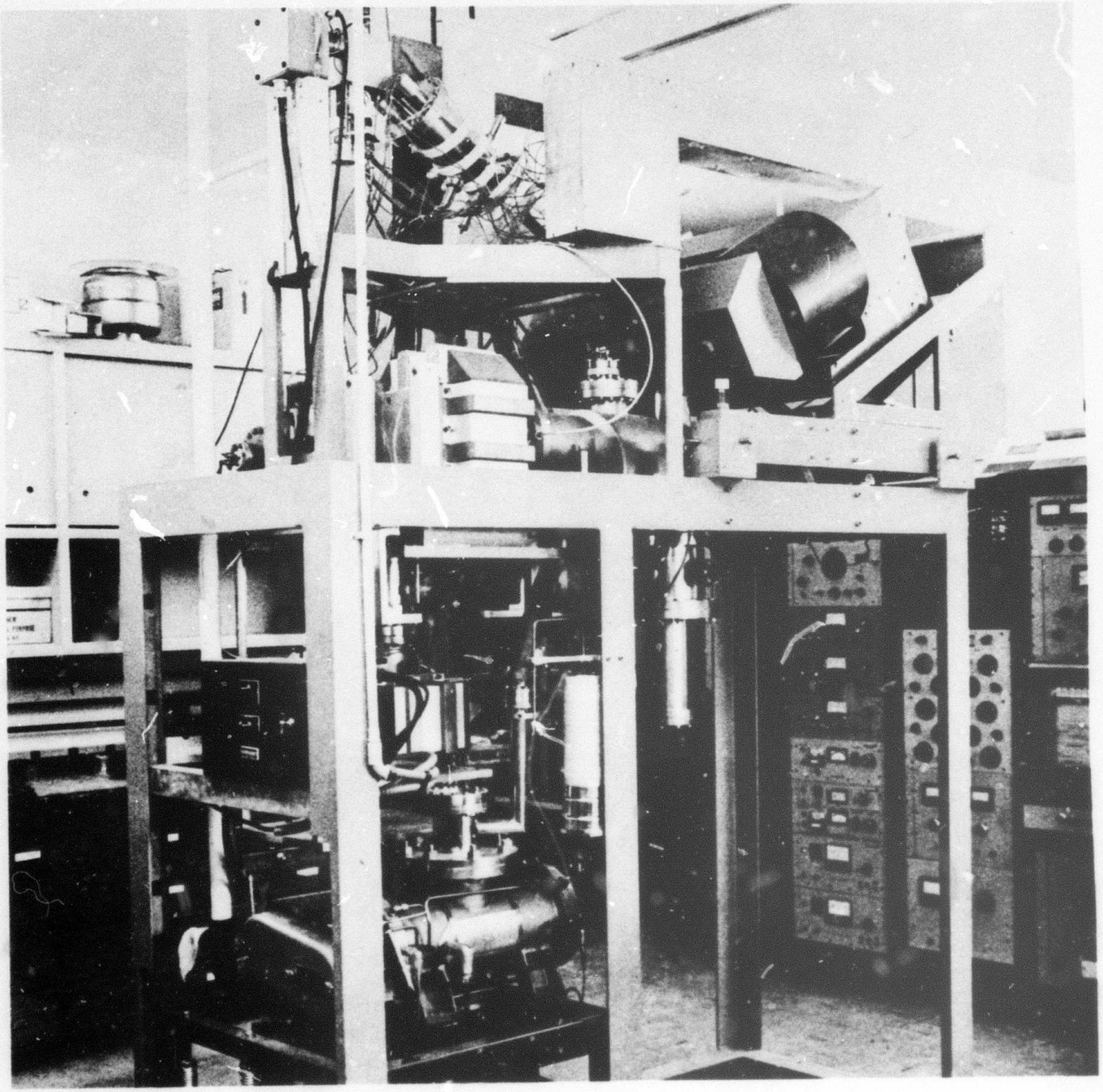

Figure 1. Photograph of 12" radius of curvature, 60° sector magnetic analyzer.

Fig. 2 Schematic diagram of magnetic analyzer showing major instrumental features.

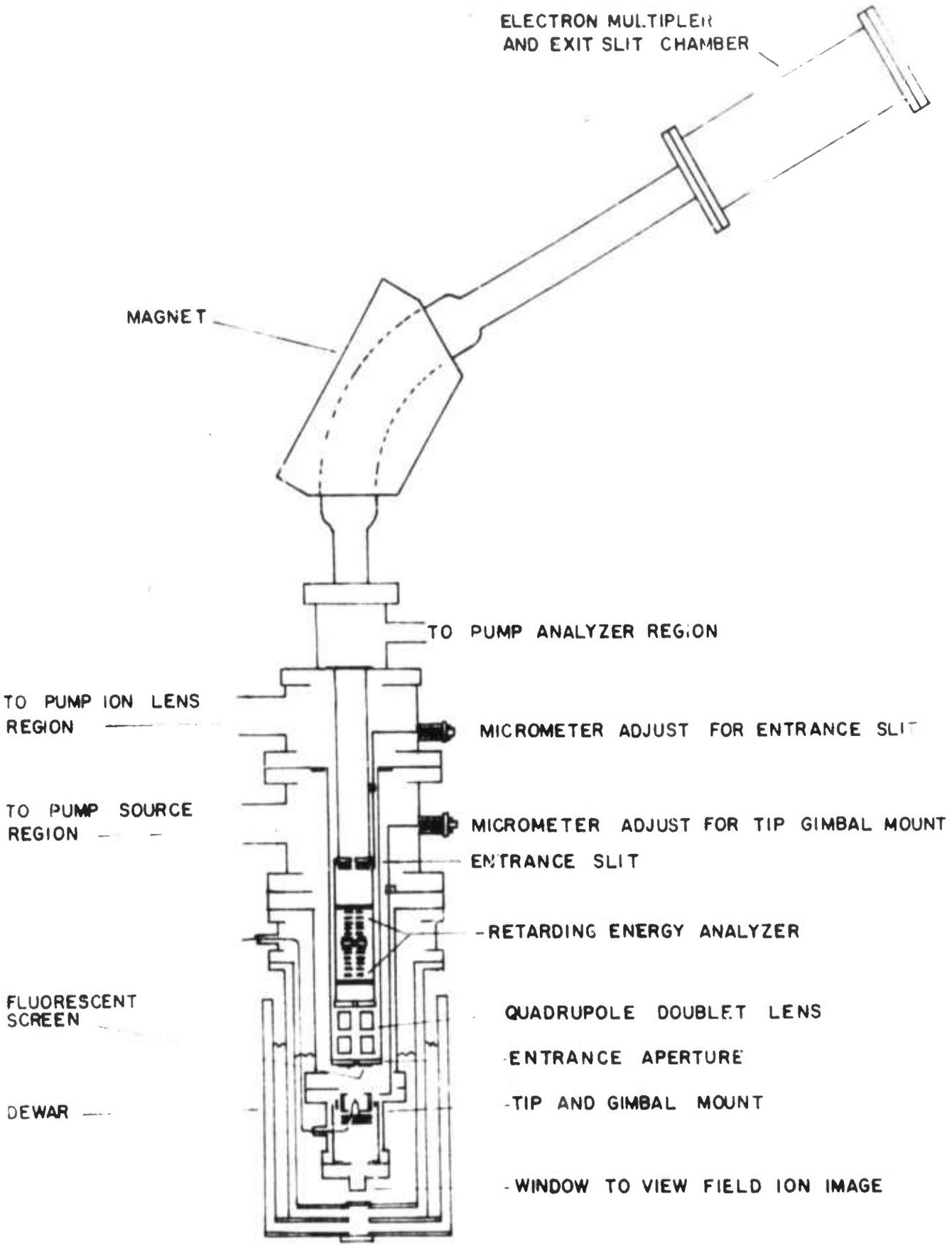

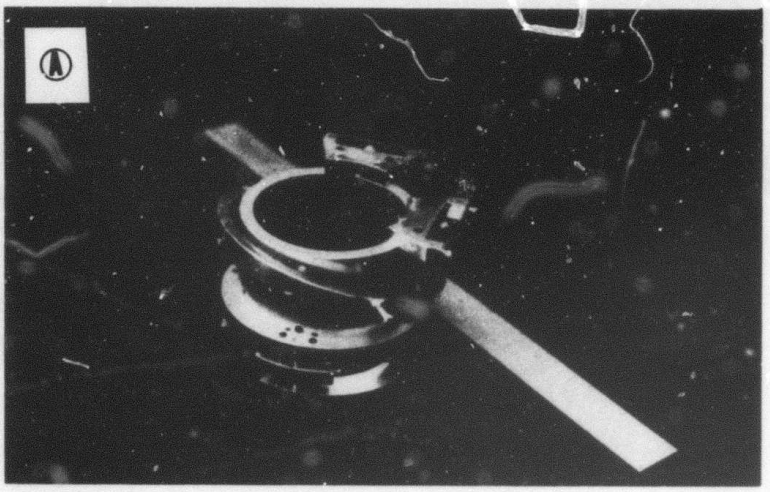

Fig. 3A Gimbals mount for field ionization source. The gimbals give two degrees of rotational freedom so that any point of the field ion image can be directed onto the entrance aperture.

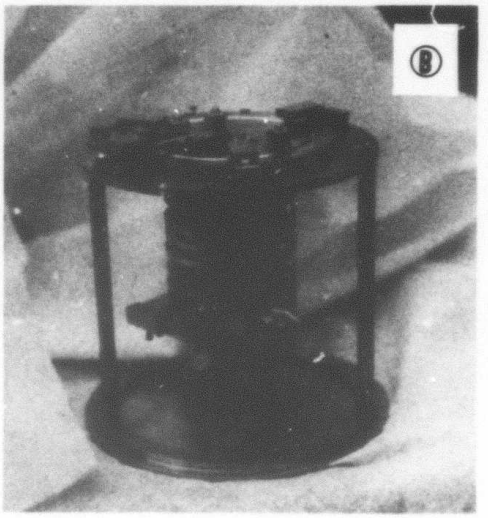

Fig. 3B Exit slit assembly of magnetic analyzer. In addition to the exit slit the assembly features a retarding lens system and a "single collector".

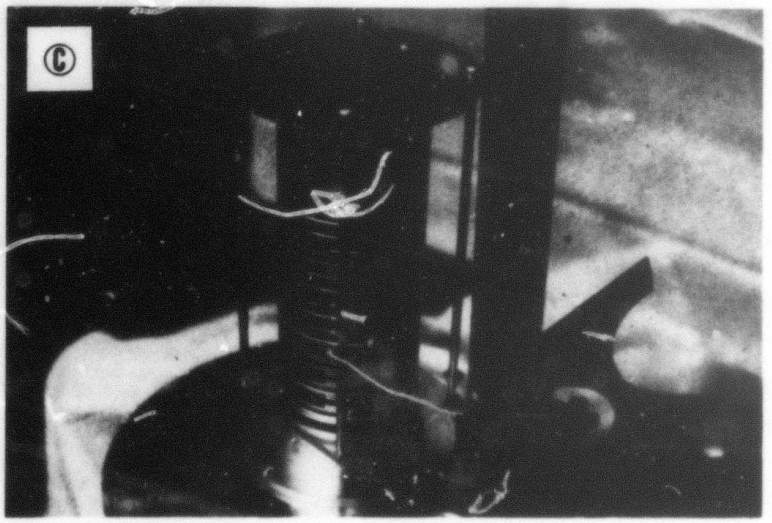

Fig. 3C 20 stage electron multiplier. The multiplier is a box and grid 20 stage electron multiplier. The dynodes are fabricated from a copper-beryllium alloy.

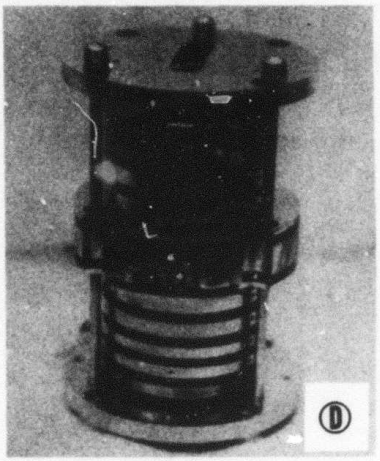

Fig. 3D Retarding lens system. The retarding plane is the thick center electrode which also contains an electron bombardment source.

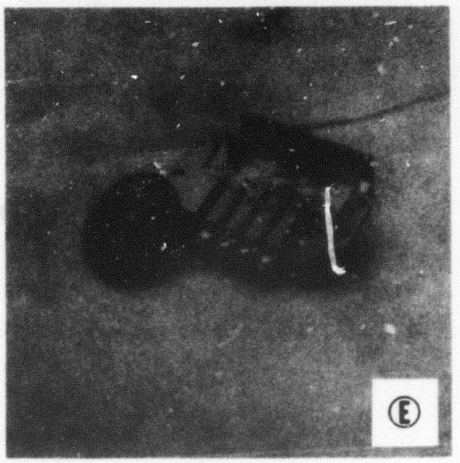

Fig. 3E Electron bombardment source.

Fig. 3F Ion lens system and entrance slit to magnetic analyzer. The lower assembly forms an electric quadrupole doublet, the central portion is the retarding energy analyzer and the upper part is the entrance slit assembly.

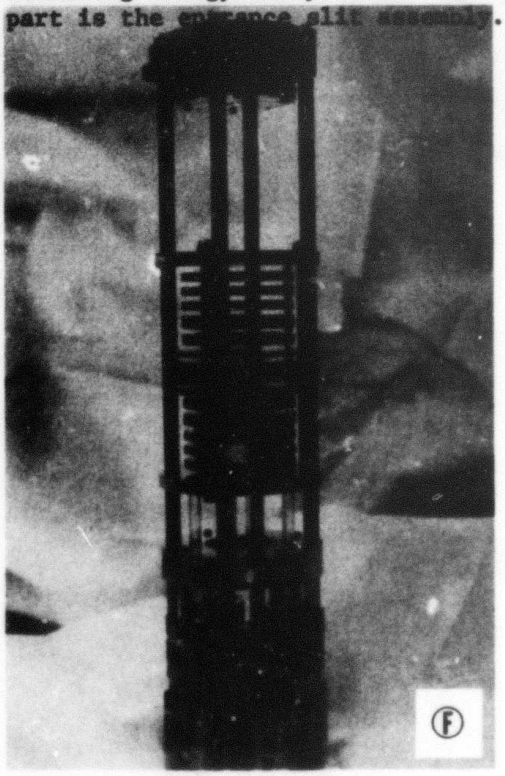

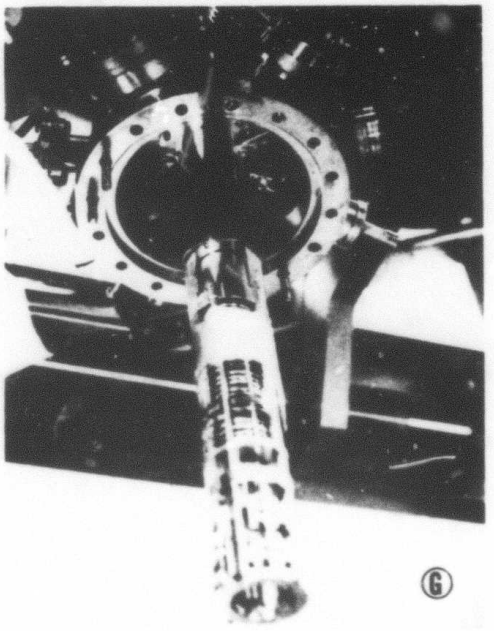

Fig. 3G Ion source positioned on the instrument.

analyzer is between the quadrupole lens and the analyzer entrance slit. The retarding lens system is shown alone in Figure 3D. The thick center electrode defines the retarding plane and it also contains an electron bombardment source used for instrument calibration, measurement of background composition and work with neutral beams. The electron bombardment source is shown in greater detail in Figure 3E.

The elements of the lens are shielded by several guard rings which constitute eight of the electrodes seen in Figures 3D and 3F. The quadrupole-filter lens assembly is mounted on a common frame and rigidly aligned with the analyzer entrance slit to better than 0.001 inch.

Ions entering the retarding lens with an energy $V_o - \Delta E$ (where V_o is the potential of the emitting surface and ΔE is the "energy deficit" from this potential) are brought to a low energy image on the retarding plane and are transmitted through the plane if their energy is greater than the potential of the plane. Transmitted ions are then accelerated by the upper segment of the lens and focused on the magnetic analyzer entrance slit. The beam geometry through the quadrupole doublet and retarding lens is illustrated in Figure 4. The potentials of the electrodes labeled "focus" determine beam convergence. The design of the analyzer has proceeded from the work of Soa[10] on the three element immersion lens and subsequent development of the "filter lens" by Simpson.[11] In short, the lens consists of two immersion lenses back to back; since a focused beam would be obtainable from zero energy ions originating at the retarding plane the converse motion is possible, i.e. retardation of the quadrupole image to a zero energy image. Ions passing through the retarding plane are then accelerated and refocused onto the magnetic analyzer slit by an immersion lens operated in standard configuration. Beam coherency is greatly aided by the small emitter size which eliminates abberation factors. Alignment and electrode spacing are critical to proper

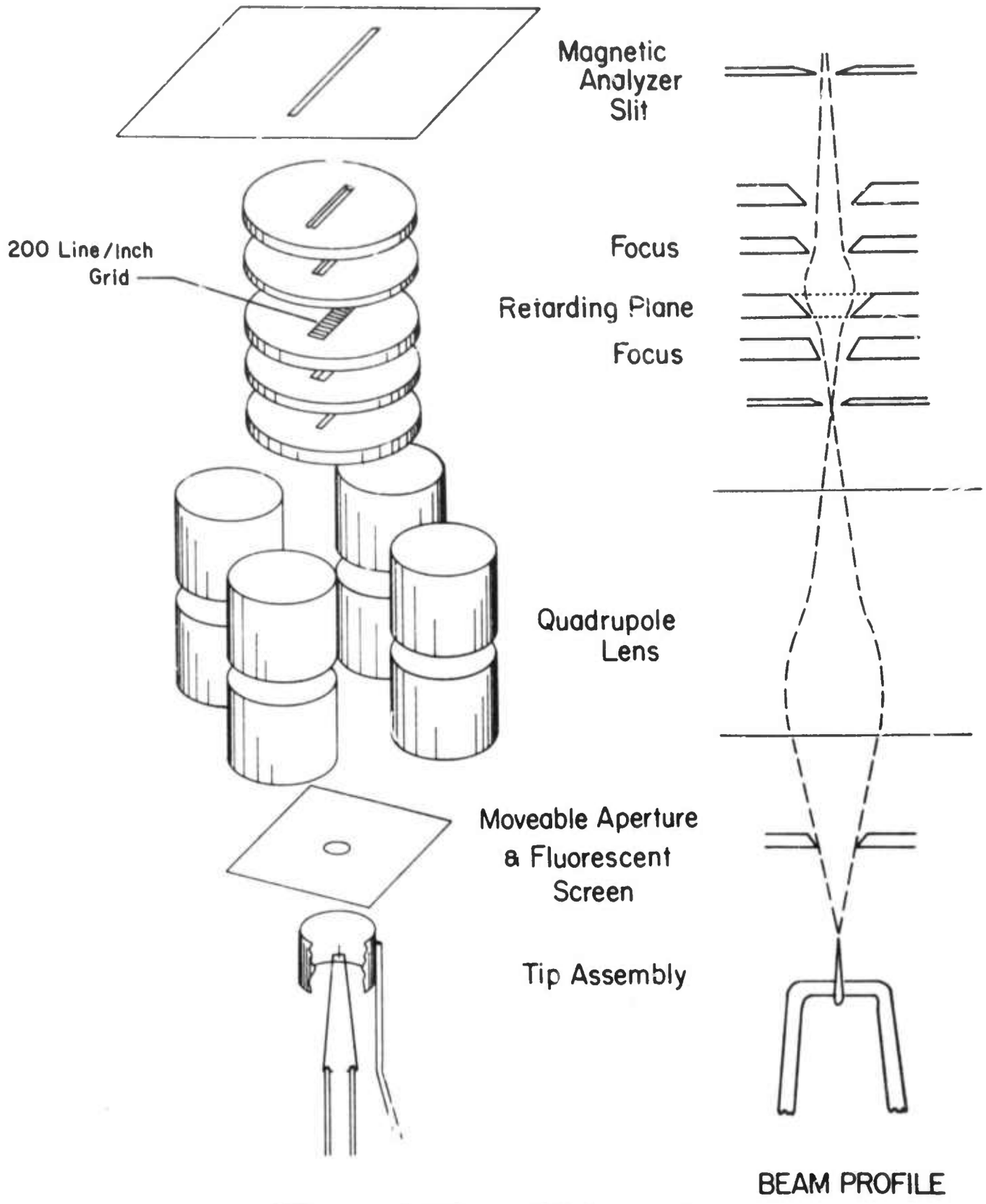

Fig. 4 Schematic drawing of ion lens system and beam profile.

functioning, hence ruby balls positioned in accurately jig bored holes are used as element spacers. The energy resolution of the device is limited about equally by the potential saddle formed at the retarding plane and optical-transmission effects to approximately 1/10,000.

These effects also limit the energy range of the retarder. However, the effective range is more severely limited by the (adjustable) bandpass of the magnetic analyzer. Because of this and the inherent limitations of integral analyzers in resolving small differential intensity changes, the use of the retarder is restricted mainly to calibration of the energy of some prominent feature of the spectra. By contrast, the differential analysis provided by the magnetic analyzer gives much better distribution detail over a wide energy range with similar resolution. The value of differential analysis is to emphasized; retarding analysis is inadequate for observing details in energy spectra as has been exemplified in many instances.

After passing through the magnetic analyzer, the ions pass through the exit slit of the mass spectrometer. The exit slit is rotatable from outside the vacuum system. This rotation allows for alignment of the entrance and exit slits for maximum resolution and transmission. This feature is unique to this instrument. Rotation is accomplished by a bellows sealed linear motion feedthrough via a linear bearing and converted to rotation about the beam axis by a wedge fastened to a spring loaded stage free to move on a ruby ball race. The exit slit assembly shown in Figure 3B also contains a "single collector" for direct measurement of the ion beam current. In addition, there is a second retarding energy analyzer for analyzing the ion beam after passing through the magnetic sector. This has distinct advantages in certain situations and verifies the results of the analyzer in the source region.

C. Output

The ion beam is then incident upon a 20 stage copper-beryllium dynode electron multiplier shown in Figure 3C. The dynode holders are constructed of annealed 50% iron - 50% nickel alloy for magnetic shielding. The dynodes were activated to give a controlled beryllium oxide surface layer which gives the electron multiplier excellent stability and a gain of about 10^8 at 150 volts/stage. The multiplier as well as the ion lens and vacuum chambers were designed and constructed by the principal investigators and the Physics Department shop at The University of Alabama.

The magnet of the differential analyzer is field regulated by using a rotating-coil gaussmeter for field sensing. The gaussmeter output is signal-processed and used to drive a well regulated magnet current supply built by the principal investigators. The field stability is better than a part in 10^5.

The differential energy analysis of the ion beam is performed using the dispersion of the magnetic field. Ion energy deficits are measured by variations of the ion acceleration voltage i.e., by applying a negative potential to the positively charged tip. The tip potential can be as high as several thousand volts and the negative voltage added varies from 0 to 100 volts. For data acquisition the negative potential added is sychronized by the sweep voltage of a multichannel analyzer (MCA) operating in a multiscaler mode. Hence, the energy deficit, ΔE, is proportional to the channel number of the MCA and the distribution can be repeatedly scanned and stored in the MCA. This gives considerable statistical improvement in the data as well as a convenient data format.

To accomplish this a special electronics unit has been designed and constructed. A block diagram of the unit is shown in Figure 5. The MCA operates from ground potential and the negative voltage to be added to the

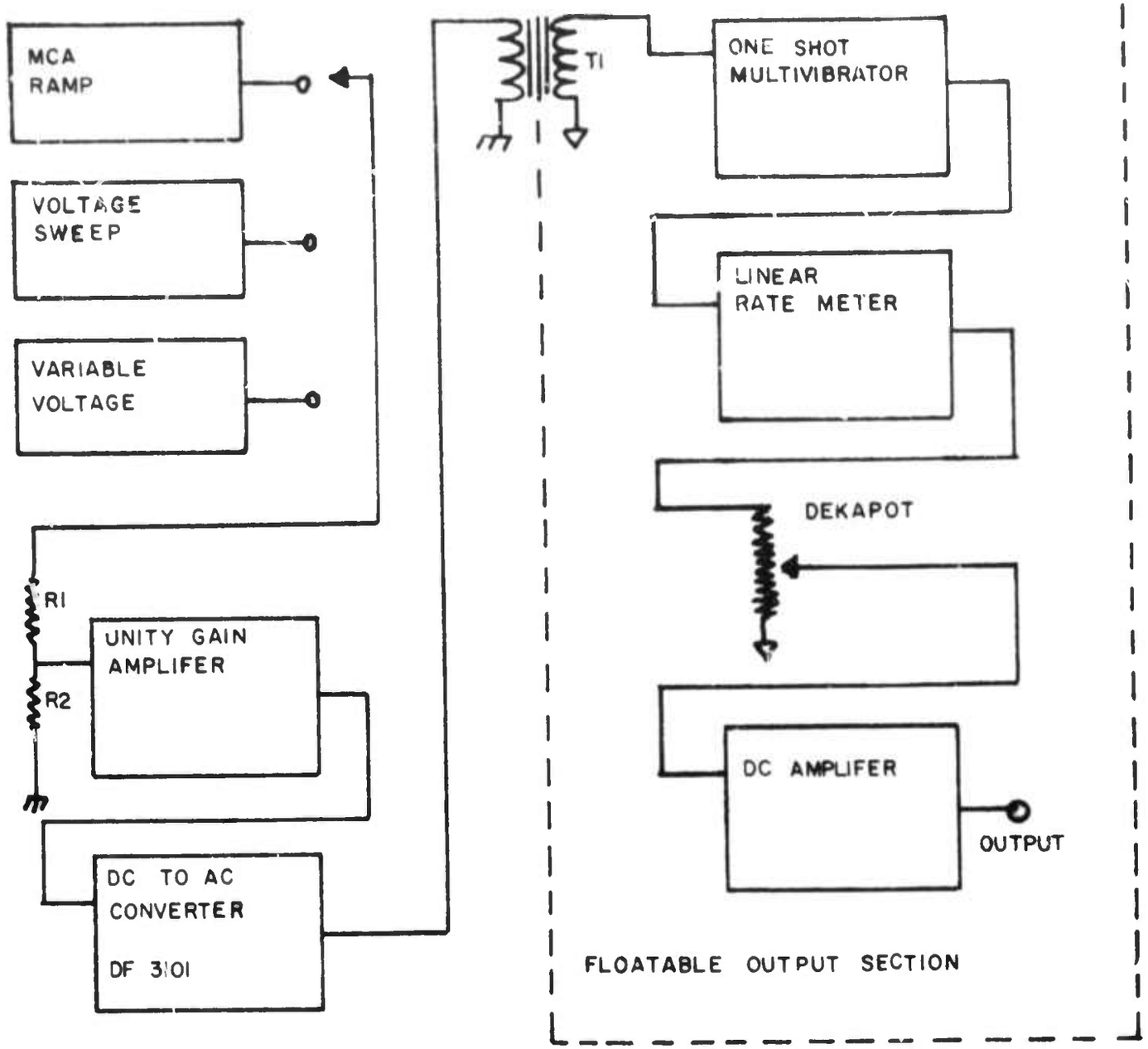

CHASSIS GROUND

OUTPUT COMMON

T1 - WX 4298F

R1, R2 - 510kΩ

Fig. 5 Block diagram of programmable isolated D.C. amplifier.

acceleration voltage is referenced to the tip voltage, hence an electrically isolated DC to DC converter is required. It was convenient to build some other operating modes into the device; voltage sweep with variable rate and manually variable voltage. These features allow data to be taken on an X-Y recorder and for rapid uncalibrated inspection of the energy deficit spectra on a time base. The inputs supply 0 - 10V which is impedance matched to the DC to AC converter. The North Hills DF 3101 puts out a 0 to 5KHz pulse rate for the 0 to 5 volts input and drives the pulse transformer through an emitter-follower amplifier. The secondary of the transformer is connected to a vacuum tube one shot multivibrator and then to a linear ratemeter which gives a DC voltage proportional to the pulse frequency. The output of the ratemeter is appropriately divided by a 100KΩ Dekapot. The signal is then amplified by a DC amplifier of low output impedance with gain adjusted so that full scale output is 100 volts. Any other precision output full scale can then be selected by appropriate setting of the Dekapot divider. The unit gives better than 1% linear relationship between input and output voltages.

The same system used for the differential analysis is used for retarding analysis except that the varying voltage is applied to the retarding plane electrode.

In either mode the data can be displayed as a DC current using a vibrating capacitor electrometer to measure the electron multiplier current. A sweep generated by the device previously described is used to drive the horizontal axis of an X-Y recorder with the vertical axis driven by the electrometer output.

D. Ion Image

The field ion image can be viewed with an image intensifier and an optical system. The field ion image is formed on a fluorescent screen in the

plane of the entrance aperture to the quadrupole lens. This image is then focused on the photocathode of an EMI 9694 image intensifier. For optimal light interception it is desirable to have the first lens of the optical system as near as possible to the field ion image. This necessitates mounting a lens in the cryogenic fluid near the viewing window at the bottom of the ion source. The focal properties of this lens will be affected by the cryogenic fluids used. To insure appropriate overall focal properties a computer program was written that would solve for the distances and focal lengths of a four element lens system subject to the constraints of the experimental system. The optical system and the dewar are shown in Figure 6. The position of the last lens in the system is adjustable to accomodate the changes in the first lens' focal length. The overall magnification of the system is about 1.5.

E. Cryogenic System

The cryogenic system has been recently implemented. The experimental dewar was especially designed and constructed by us (shown in Fig. 6). The dewar consists of two reservoirs with a common vacuum and indium gasket sealed windows. The header shown above the dewar has high voltage feed throughs and a transfer interlock as well as pumping ports and level sensing leads. The heat leak to the cryogenic fluid is minimized by dynamic cooling of the spectrometer flange contiguous to the dewar with liquid nitrogen. Under these circumstances the heat input to the fluid is approximately two watts with a subsequent boil off of liquid hydrogen of about 1/4 liter/hr. Liquid helium can be used as a coolant but sustains a loss rate of two liters per hour. While this is an acceptable static loss rate, the vaporization of liquid helium in cool down and transfer becomes quite expensive. For most experiments liquid hydrogen is preferable to liquid helium. The necessity

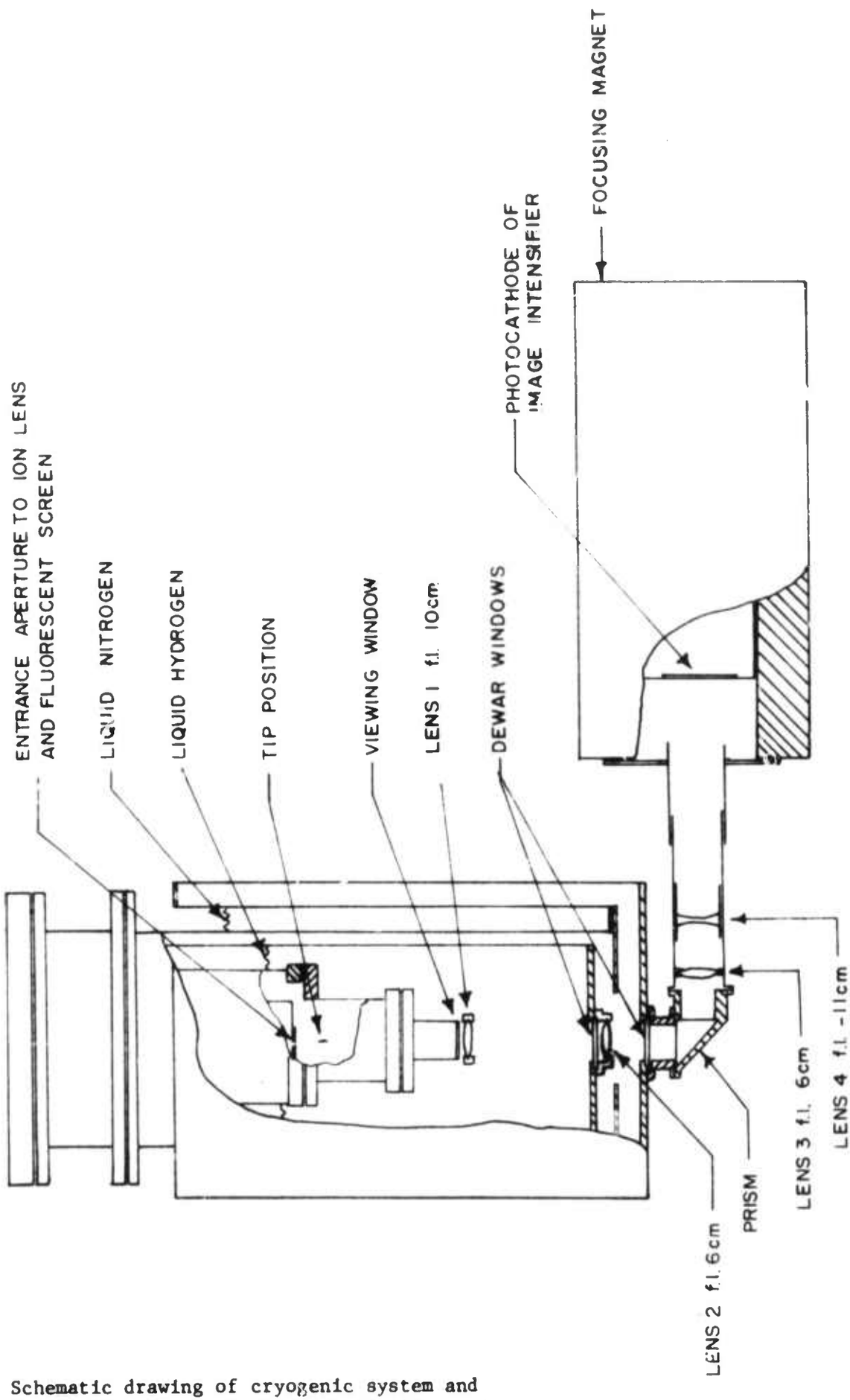

Fig. 6 Schematic drawing of cryogenic system and the optical system for viewing field ion image.

for substrate cooling has been extensively discussed[2] in terms of stability and sample purity.

IV. EXPERIMENTAL RESULTS

A. Instrumental Resolution

Equipment performance is demonstrated in Figure 7 which plots the mass spectrum of ions with nominal mass to charge ratio of 28. This plot was obtained using the electron bombardment source to produce ions from residual gas and recorded with MCA by scanning the ion acceleration potential as previously described. The figure demonstrates the sensitivity and resolution capabilities of the differential analyzer; the energy resolution (equal to the mass resolution) is better than one part in six thousand. A significant fraction of the peak width is due to an inherent energy spread in the electron beam source. The total pressure in the spectrometer was in the 10^{-10} Torr range, thus demonstrating good instrumental sensitivity in view of the low partial pressure of the components of the mass 28 spectrum.

B. Observation of Secondary Structure

Figure 8 illustrates an energy distribution for hydrogen as imaging gas on a tungsten substrate. The distribution although not well resolved and taken at room temperature shows the secondary structure clearly. The ions originated from several surface atoms on a "rough" area off the 110 plane. The ill resolved secondary structure is characteristic of rough areas; a smooth region such as the 110 plane produces a greater peak to valley ratio. The validity of this conclusion depends on surface condition, surface orientation and area viewed.

C. Main Peak Structure

The main peak shows structure when viewed under high resolution. Figure 9 gives a more highly resolved energy distribution taken with retarding analysis

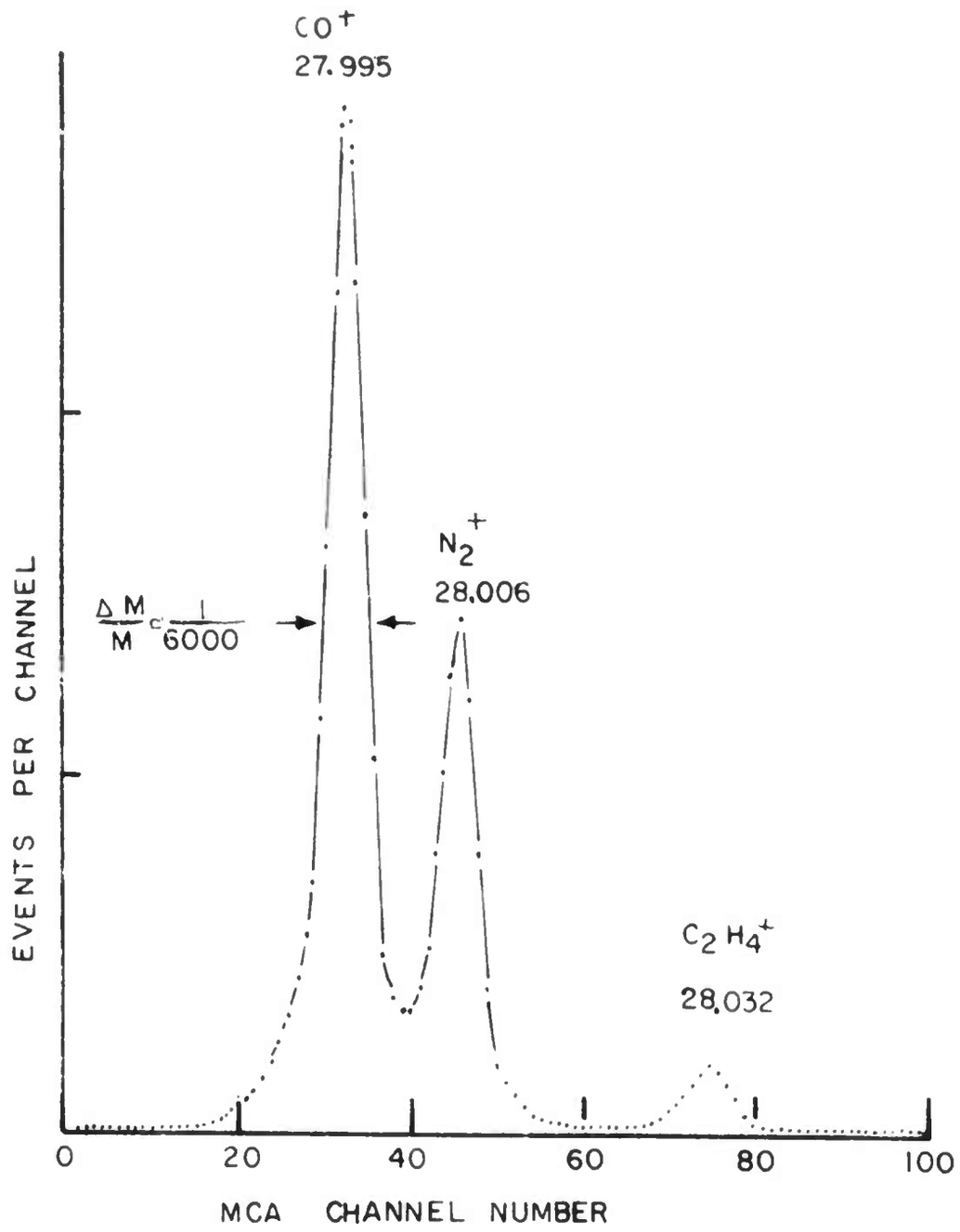

Fig. 7 Plot showing dispersion capabilities of magnetic analyzer, The horizontal axis is MCA Channel number which is proportional to mass and the vertical axis is the ion intensity per channel. The full width at half maximum corresponds to a resolution of $\Delta M/M \sim 1/6000$.

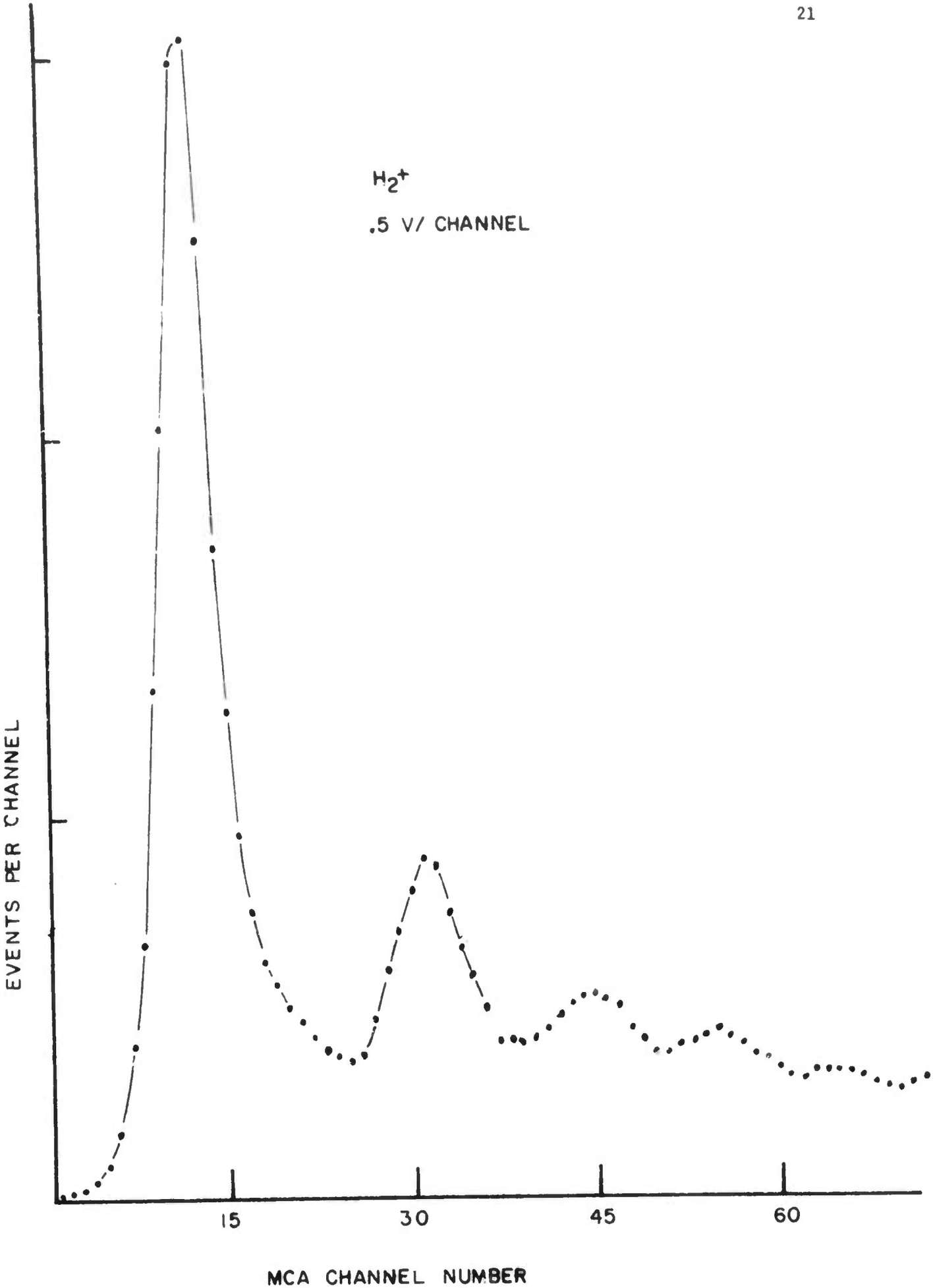
H_2^+
.5 V/ CHANNEL
EVENTS PER CHANNEL
15
30
45
60
MCA CHANNEL NUMBER

Fig. 9 High resolution retarding analysis of primary peak in the H_2^+ field ionization energy spectra.

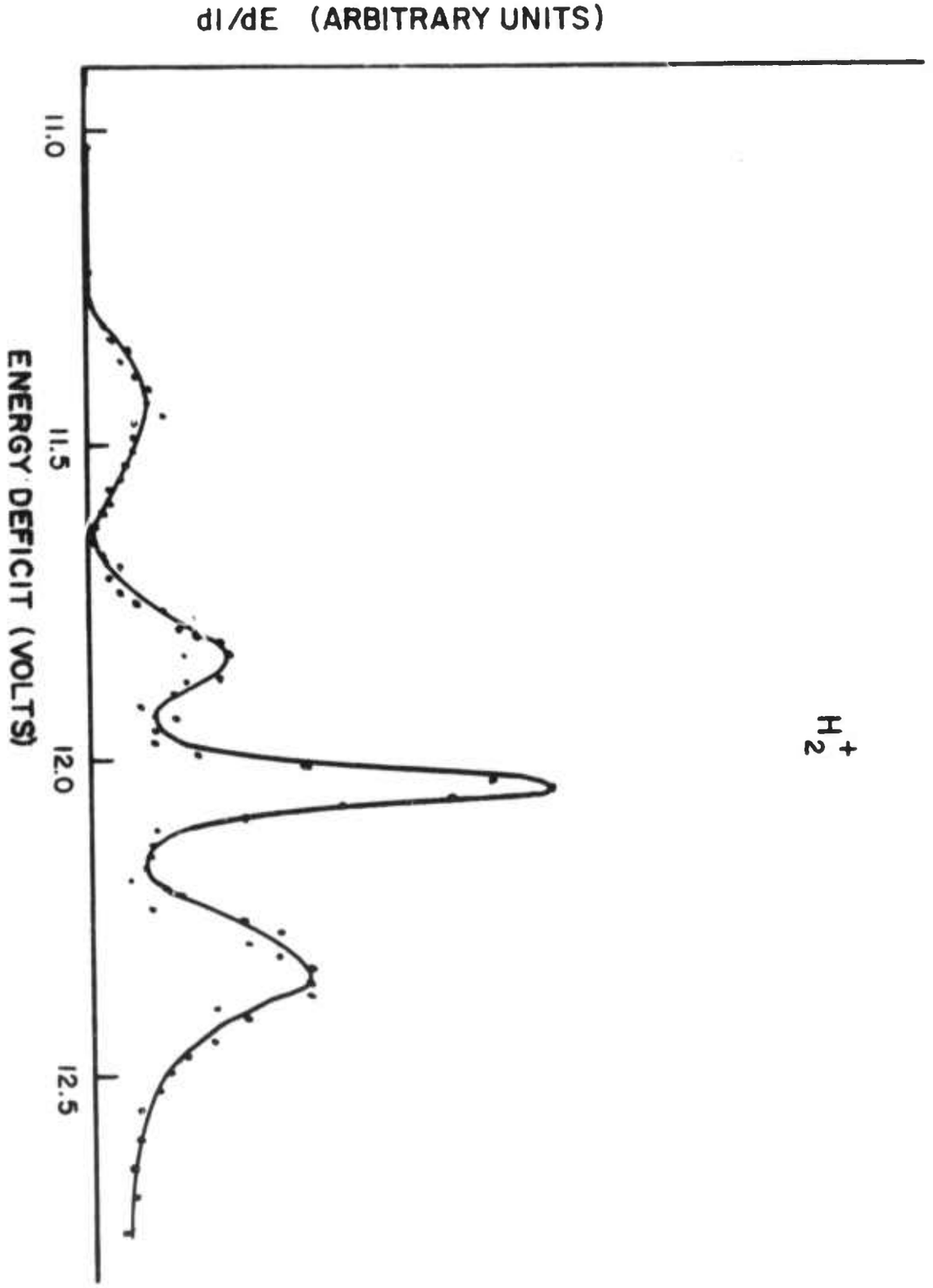

under poorly specified surface conditions. In particular this result does not compare directly with calculated surface or bulk density of states for the substrate material. Further data at low temperatures will better specify this structure which is highly specific to surface location and condition.

D. Distribution Onsets

The distribution onsets, determined by energetic alignment of the ionizing atom with the substrate Fermi level should occur to first order at an energy deficit $\Delta E = I - \phi$ where I is the ionization potential and ϕ is the work function of the surface (experimentally ϕ becomes an instrumental parameter due to exact cancellation of ϕ by the contact potential difference between the emitter and ground). This relationship has been verified experimentally for several gases in Figure 10 where a linear relationship between I and onset energy deficit is found.

The remarkable invariability of this rule is simply due to the fact that the energy of the metal-ion system does not change during the field ionization process. The increase in the metal energy due to addition of the tunneling electron is matched by the decrease in potential energy of the ion, observed as the energy deficit. Hence, the technique is valuable for measurement of ionization potentials of large molecules. In addition, the formation energy of any ionic species formed by field ionization can be found by regarding the onset energy deficit as an appearance potential in the same sense as in electron impact and photon impact experiments. This has been pointed out by us in the case of H_3^+ formation[3].

These results also help to establish the role of surface-atom interaction and molecular polarization in field ionization energetics. This work is to be published and is currently being written up.

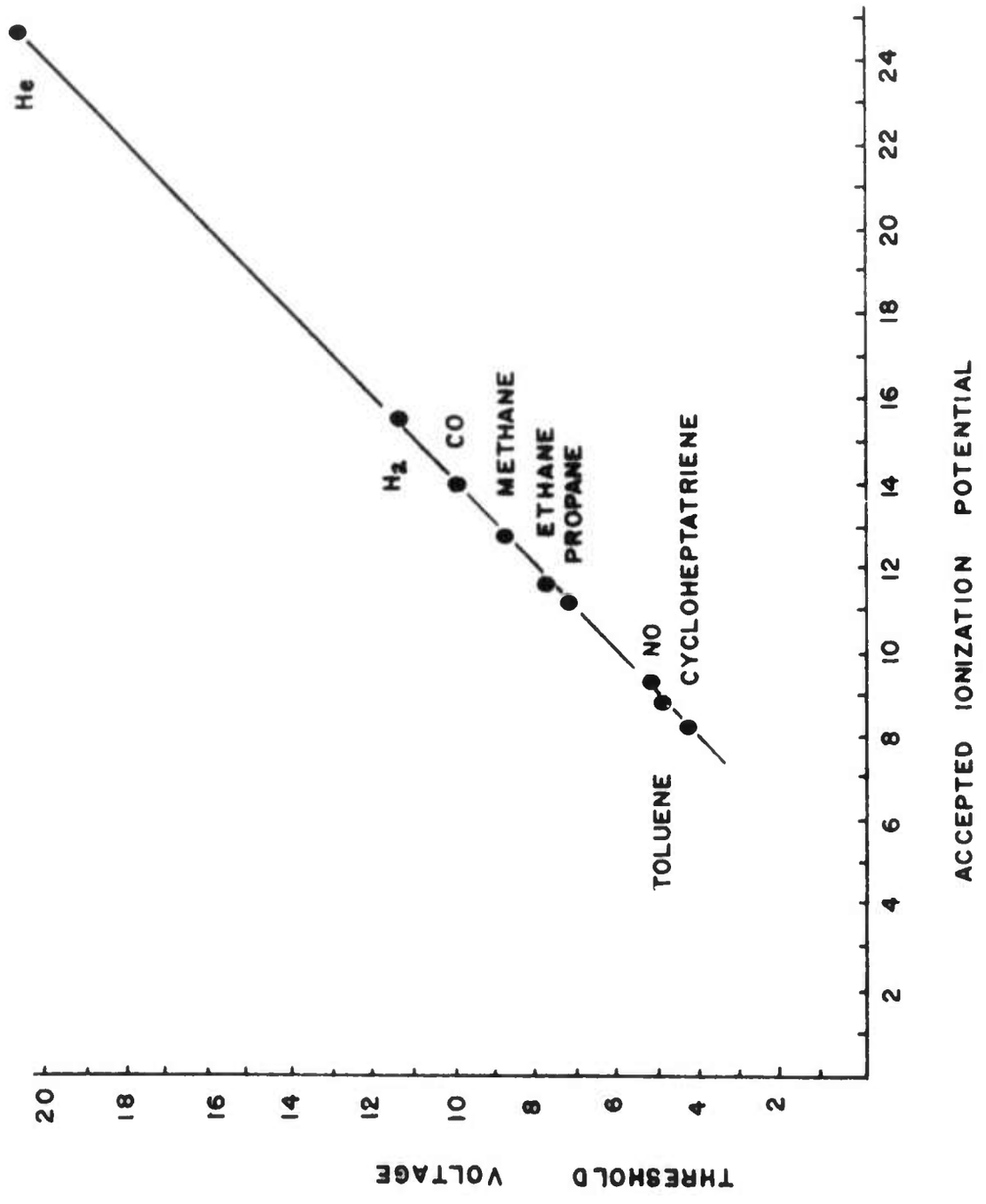

Fig. 10 Plot showing linear relationship between field ionization onset energy and accepted ionization potential.

V. CONCLUSION

Instrumental problems have been resolved and experimental work is encouraging. The current results imply that careful experiments on energy spectra above clearly delineated surface areas yield relationships between the spectra and surface structure. These results should be extended to materials other than the transition metals currently in use. Alloys form a particularly interesting and important system to be experimentally parameterized. In addition, semiconductor surfaces should be studied. Results should involve the presence of the semiconductor band gap and clarify the expected relation between spectra and band structure. Experiments are also planned involving field ionization of cesium and barium. Because of their low ionization potentials these elements would ionize very near to the surface. The strong interaction with the surface at near distances would manifest itself in the energy spectra.

VI. REFERENCES

1. Original proposal to grant AFOSR 74-2726, "Characterization of Surfaces on an Atomic Scale by Field Ionization Energy Spectra" by A. J. Jason and A. C. Parr.

2. E. W. Müller and T. T. Tsong, Field Ion Microscopy (Elsevier, New York, 1969).

3. A. J. Jason, Phys. Rev. 156, 266 (1967).

4. T. Utsumi and N. V. Smith, Phys. Rev. Letters 33 1294 (1974).

5. J. Appelbaum, private communication, to be published.

6. E. W. Müller and S. V. Krishnaswamy, Surface Sci. 36, 29 (1973).

7. E. W. Müller and T. Sakurai, J. Vac. Sci. Tech. 11, 878 (1974).

8. G. R. Hanson, G. E. Humes, and M. G. Inghram, Chem. Phys. Letters 27, 479 (1974).

9. G. R. Hanson, to be published, J. Chem. Phys.

10. E. A. Soa, Jenaer Jahrbuch 1959/1 (Carl Zeiss, Jena 1959), p. 115.

11. J. A. Simpson, Rev. Sci. Instr. 32, 1283 (1961).

Appendix: ENERGY SPECTRA OF ORGANIC MOLECULES IN FIELD IONIZATION

ENERGY SPECTRA OF ORGANIC MOLECULES IN FIELD IONIZATION*

Andrew J. Jason and Albert C. Parr
Department of Physics and Astronomy
The University of Alabama
University, Alabama 35486

ABSTRACT

Field ionization energy spectra of toluene, cycloheptatriene and phenol are reported. Details of the spectra are correlated with molecular properties. The implications of the observation for analytical work are discussed.

INTRODUCTION

Field ionization has proven to be a useful tool in the mass spectrometric study of organic molecules. This paper presents data which suggest techniques for extending the information obtainable from field ionization mass spectrometry. High resolution energy analysis of field ionization products provides energy spectra which correlate with molecular properties. Such data can potentially provide information useful in interpreting mass spectra as well as in studying the field ionization of molecules.

Energy analysis of organic molecular ions created at a field emitter has established a linear relationship between appearance potentials measured by various techniques and energy distribution onsets.[1-6] Specifically, for the parent ion, with ionization potential I, a first order theory of distribution onsets[1] gives the onset energy deficit, ΔE (i.e. the ion energy as observed referenced to the potential applied to the emitter), as[7] $\Delta E = I - \phi$

where ϕ is an instrumental quantity which can be determined by reference to a calibration sample such as hydrogen. Fragment onsets also relate to accepted appearance potentials for field ionization of hydrogen and further details of the dissociation process are apparent in the spectra.[8,9] We here present initial results which further demonstrate the relationship of the energy spectra to molecular structure. In addition to a characteristic onset the width and structure of the energy distributions relate to molecular properties. High resolution results on the energy spectra of toluene, cycloheptatriene and phenol are given and compared to the results of photoionization, photoelectron spectroscopy, and electron bombardment techniques.

EXPERIMENTAL

Energy analyses were performed using a 60°, 12-inch radius of curvature, magnetic analyzer. The practical energy resolution obtainable with this instrument is about 1 part in 10,000. The instrument features a bakeable ultra high vacuum system, dual gas inlet, and temperature controlled source (from 450° C. to liquid helium temperatures). An electron bombardment source is included in the instrument for use as a conventional mass spectrometer. Ions in this experiment originated from a small area of a single tungsten tip. The ions from an included angle of approximately 7° are focussed by an electric quadrupole doublet onto the entrance slit of the magnetic analyzer. A 20 stage particle detector is capable of detecting individual events or an integrated current. Since low intensities are obtained using single tip emitters, a multiscaler was used to acquire digital data. The address of the multiscaler was proportional to a slow sweep voltage

applied to the emitter as a small deficit of the accelerating potential. After many sweeps a statistically significant plot of the differential energy distribution was obtained.

The samples used in this experiment were research grade materials and were vacuum distilled before introduction to the system. Electron bombardment analysis was used to check sample purity. Background vacuum in the instrument was of the order of 10^{-8} Torr or better and experiments were performed at room temperature. Ion energies were of the order of 1 KV with an applied field of about 10^{8}V/cm. At the fields used, ionization far from the surface was not appreciable and fragmentation was negligible. The small tips used here provided very low intensities (of the order of 50-500 ions/second) so that digital accumulation was necessary.

RESULTS AND DISCUSSION

The existence of an onset energy deficit is graphically depicted in Fig. 1 which plots the number of ion counts of the parent ion of a phenol sample versus a differential voltage applied to the accelerating voltage. The horizontal scale is hence related to the energy deficit by an additive quantity. Data was taken by obtaining a field ionization beam and accumulating over repetitive 20 V sweeps at constant magnetic field to obtain the peak on the right. The field ionization beam was then turned off and the electron beam source activated. Maintaining the magnetic field and static portion of the accelerating potential constant, data was again accumulated by sweeps over the energy deficit. This produced the peak on the left. The measurement of onset separations in this plot (approximately 4.2 volts) is

not strictly a measurement of critical energy deficit because of small effects due to repeller and drawout potentials (~ 0.1 volt) encountered in the electron beam source. This uncertainty can best be overcome by use of retarding techniques[3] which calibrate the energy deficit scale to within the additive instrumental quantity ϕ as discussed in the introduction.

Figure 2 gives the energy distribution for toluene on a smaller energy scale than that of Fig. 1. The energy scale has been set so that the observed critical onset in volts numerically equals the accepted ionization potential, 8.82 eV.[10] The peak rises to its maximum value in about 0.6 volts from onset and subsides into a long tail. The width of the peak is approximately 1 volt at half maximum, considerably broader than the instrumental resolution which for these cases is of the order of 200 millivolts. The width is interpreted as due to a combination of: (1) "inherent" width due to factors involving the metal surface structure and tunneling probability (2) width due to the involvement of excited ionic states in the field ionization process. We believe that much of the structure in the distribution is due to this latter effect.

Figure 3 schematically portrays the presumed role of upper states in the spectra. Figure 3a gives the general features of a field ionization energy distribution for ionization to an upper state. The general form of this peak as depicted has been experimentally verified.[7,12] A sharp rise at onset is featured with a gradual tail at higher energy deficits due to a diminished ionization probability for ions originating farther from the surface. If a single excited state exists at an energy ϵ above the ionic ground state, a distribution as shown in Fig. 3b would then be expected; transitions

to the excited state would produce a superimposed second peak with onset at $\Delta E = I - \phi + \epsilon$. Depending upon the value of ϵ and the inherent width of the two peaks in Fig. 3b, structure may be evident in the energy distributions. Figures 3c and 3d demonstrate a presumed correspondence of the field ionization spectra to the ion appearance spectra obtained by electron bombardment and photoionization respectively. The correspondence is determined by a change in the total ionization probability as the energetics become favorable for transitions from the ground state of the neutral molecule to the accessible states of the ion. In field ionization the parameter describing the energy balance is the energy deficit. The energy deficit equals the energy transferred to the metal via the tunneling electron and subsequent loss by the ion. For the electron bombardment and photoionization cases the corresponding quantity is the energy loss of the bombarding particle which equals the energy gained by the molecule. Figure 3b gives an idealized representation (as do Figs. 3c and 3d) which in general would not be experimentally realized. High resolution photoionization data for toluene[10], for example, shows a gradual onset with several resolved "steps". These features correspond well (with due regard for statistical significance of the data) with the structure perceptible in Fig. 2. Such structure is reproducible in repeated runs as long as instrumental stability is not taxed by excessive data accumulation times.

Figure 4 gives the field ionization spectrum of cycloheptatriene with onset at the appropriate appearance potential[10] (8.28 V). The distribution has a sharper rise than toluene and differing structure in accord with photoionization results.[10]

Figure 5 gives the field ionization spectrum of phenol. The features of this distribution compare well with photoelectron data taken by Baker, May and Turner.[13] In particular a second electronic state 0.7 eV above onset was observed by them which correlates with the unresolved structure around 10 volts in Fig. 5.

CONCLUSIONS

The parent field ionization energy distributions show structure which in part can be attributed to the vibrational and electronic excitation of the molecular ion. The ionization onsets can be measured and compared with impact data. These two attributes of the spectra can be utilized for investigations concerning the field ionization process, study of molecular structure, or as a tool in analytical work. For example, the two mass isomers, toluene and cycloheptatriene, can be readily distinguished in analysis of field ions by the difference in onset energies (0.54 volts).

Ions formed by fragmentation and surface reactions also have energy spectra characteristic of their formation process and internal structure. Fragment ions have onsets characteristic of the fragmentation energy involved and have distributions differing in shape and extent from parent spectra, a property understandable on the basis of the kinetics of fragmentation.[9] Surface reactions on the other hand such H_3^+ [8] formation or ionization from liquid layers[14] show a narrow peak indicative of ionization only very near the surface and with onsets related to formation energies. Such characteristics can be utilized in analysis work (e.g. by selective energy retardation) to simplify and aid in interpreting mass spectra.

Further investigation of the relation between field ionization energy spectra and molecular structure is being accomplished. In particular it is necessary to determine the extent to which the surface structure modifies the distribution charactersitics. For example, differences in the number of surface atoms sampled (i.e., size of the emitting surface utilized) and crystal plane viewed affect the distribution details and in some cases the species formed. Work is also necessary to establish the spectra of multiple emitters which are a necessary component of practical field ionization analysis systems.

REFERENCES

*Work supported in part by Grant AFSOR 74-2726 and in part by the Research Grants Committee of The University of Alabama.

1. E. W. Müller and T. T. Tsong, "Field Ion Microscopy: Principles and Applications", American Elsevier Publishing Corp., Inc., New York, NY 1969.

2. A. J. Jason, 13th Field Emission Symposium, Cornell University, Sept., 1966.

3. To be published, present authors.

4. A. J. Jason and A. C. Parr, Interim Technical Report AFOSR 74-2726 (1975).

5. A. J. Jason and A. C. Parr, First Annual ARPA Conference on Surface Physics, Philadelphia, Nov., 1974.

6. I. V. Goldenfeld, I. Z. Korostyshevsky and B. G. Mischunchuk, Int. Jour. Mass Spec. and Ion Physics, 13 (1974).

7. A. J. Jason, Phys. Rev. 156 (2), 266 (1967).

8. A. J. Jason, R. P. Burns and M. G. Inghram, J. Chem. Phys. 43, 3762 (1965).

9. G. R. Hanson, J. Chem. Phys. 62, 1161 (1975).

10. F. A. Elder, Thesis, Department of Chemistry, University of Chicago, 1968.

11. J. L. Franklin, et al., "Ionization Potentials, Appearance Potentials, and Heats of Formation at Gaseous Positive Ions", NSRDS-NBS-26 (1969).

12. T. T. Tsong and E. W. Müller, J. Chem. Phys. 41, 3279 (1964).

13. A. D. Baker, D. P. May and D. W. Turner, J. Chem. Soc. (B) 22, (1968).

14. A. J. Jason, R. P. Burns, and M. G. Inghram, J. Chem. Phys. 43, 3762 (1965).

FIGURE CAPTIONS

Fig. 1 A plot of the parent ion intensity for phenol per unit energy interval in arbitrary units on the veritcal scale and energy deficit on the horizontal scale. The figure illustrates the existence of a critical energy deficit and places an upper limit to instrumental resolution.

Fig. 2 A plot of the parent ion intensity for toluene per unit energy interval in arbitrary units on the vertical scale and energy deficits in volts on the horizontal scale. The energy deficit scale has been adjusted so that the critical onset energy deficit numerically equals the ionization potential in electron volts.

Fig. 3 Comparison of threshold of ionization onsets for field ionization, electron impact ionization and photoionization. The horizontal scales are the appropriate energy, i.e. energy deficit, electron energy or photon energy in arbitrary units. The vertical scales are ion intensity in arbitrary units.

a) Energy distribution of ions from field ionization. An abrupt onset at energy $I - \phi$ is followed by subsiding intensity for ionization to a single state of the ion.

b) Field ionization energy distribution like (a) except two states of the ion are accessible, the second an energy ε above the ground state.

c) The threshold low for electron impact is approximately a linear increase in intensity with energy. The accessibility of a second state at an energy ε above the ground state would cause a break in the curve and a change in slope.

d) The threshold law for photoionization is approximately a step function. In the case of two accessible states the ion intensities add to give the step structure indicated.

Fig. 4 A plot of the parent ion intensity for cycloheptatriene per unit energy interval in arbitrary units on the vertical scale and energy deficits in volts on the horizontal scale. The energy deficit scale has been adjusted so that the critical onset energy deficit numerically equals the ionization potential in electron volts.

Fig. 5 A plot of the parent ion intensity for phenol per unit energy interval in arbitrary units on the vertical scale and energy deficits in volts on the horizontal scale. The energy deficit scale has been adjusted so that the critical onset energy defici numerically equals the ionization potential in electron volts.

PHENOL m/e = 94

Figure 1

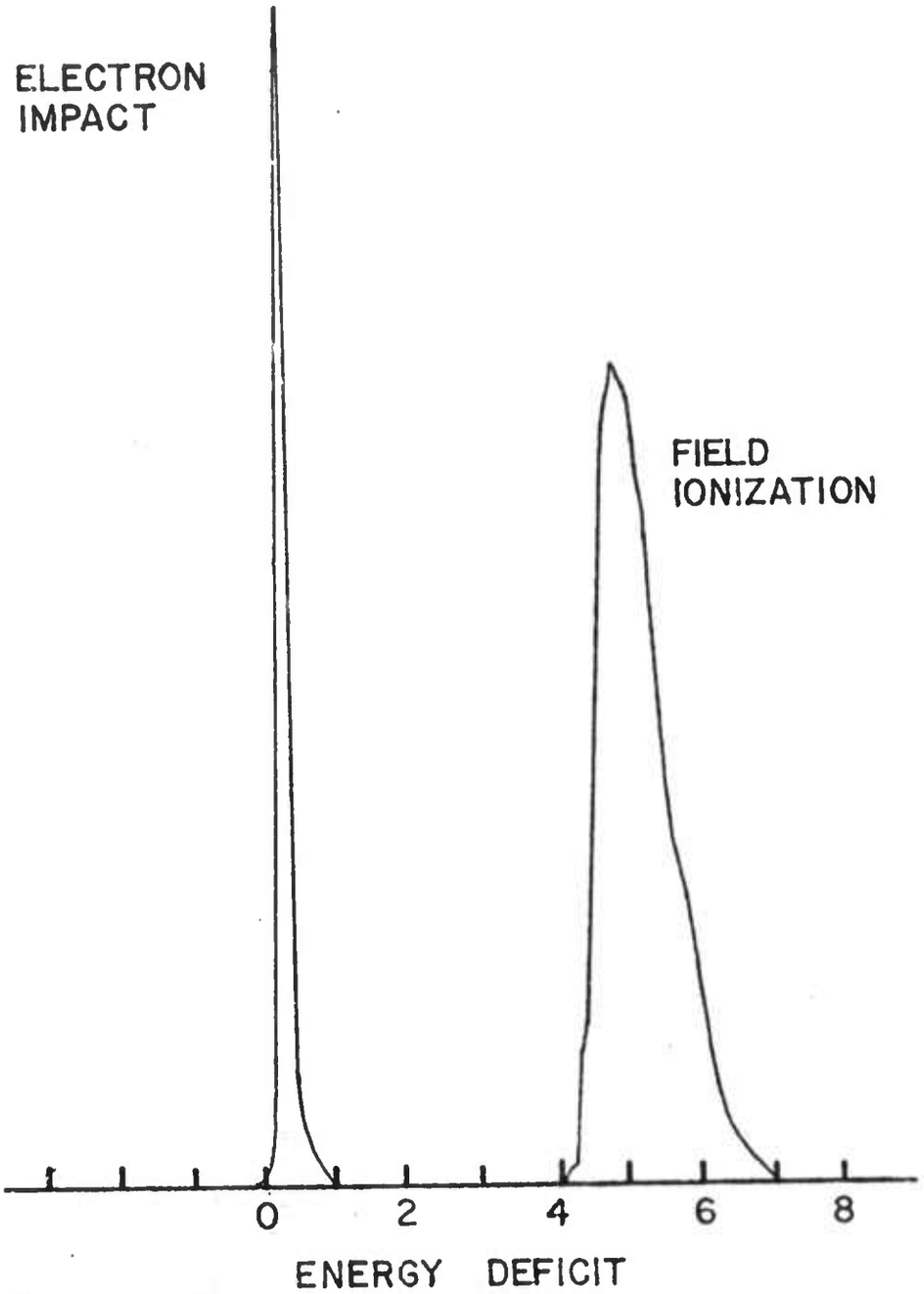

Figure 2

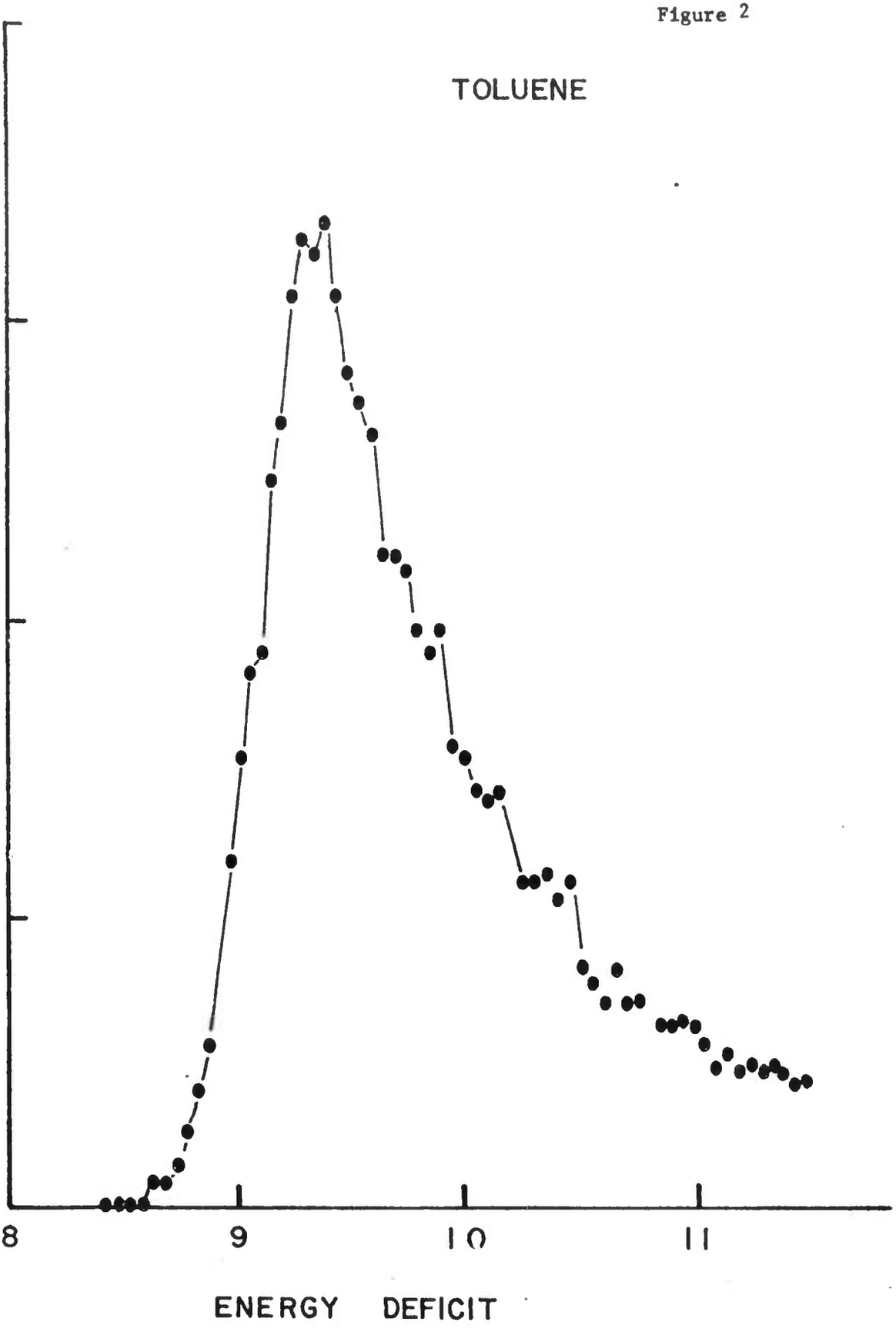

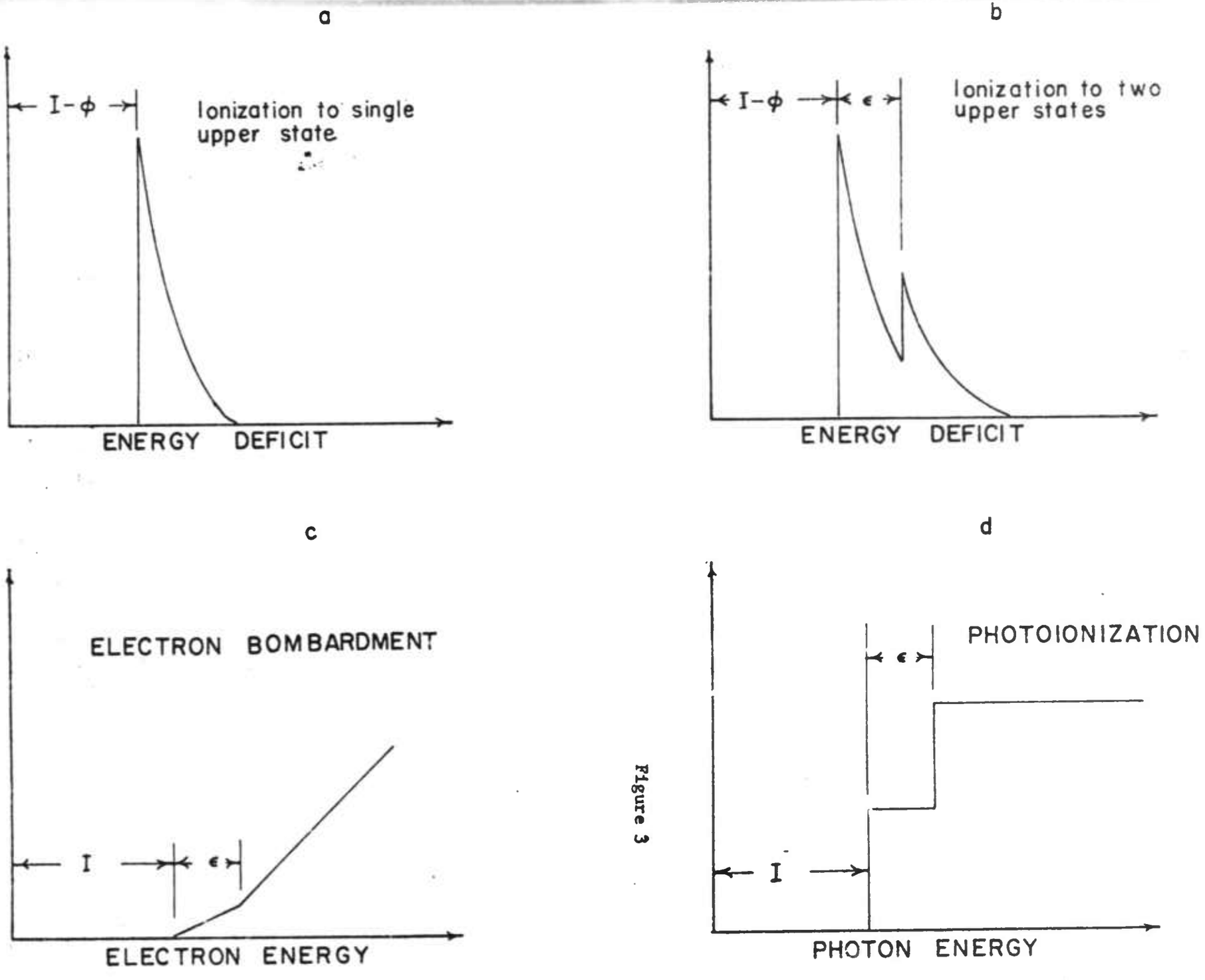
a
I-ϕ
Ionization to single upper state
ENERGY DEFICIT
b
I-ϕ
ϵ
Ionization to two upper states
ENERGY DEFICIT
c
ELECTRON BOMBARDMENT
I
ϵ
ELECTRON ENERGY
d
PHOTOIONIZATION
ϵ
I
PHOTON ENERGY

Figure 3

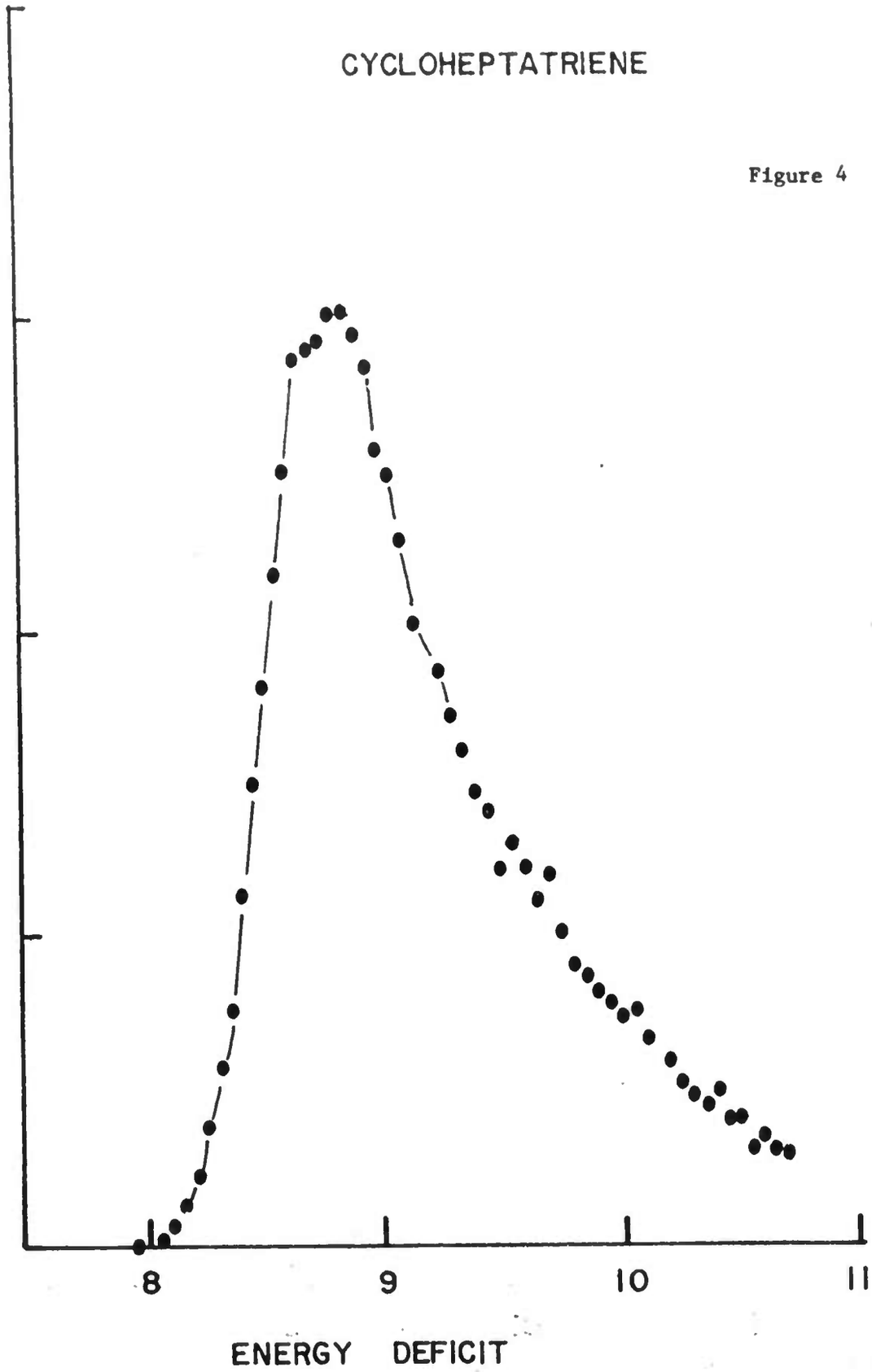

Figure 4

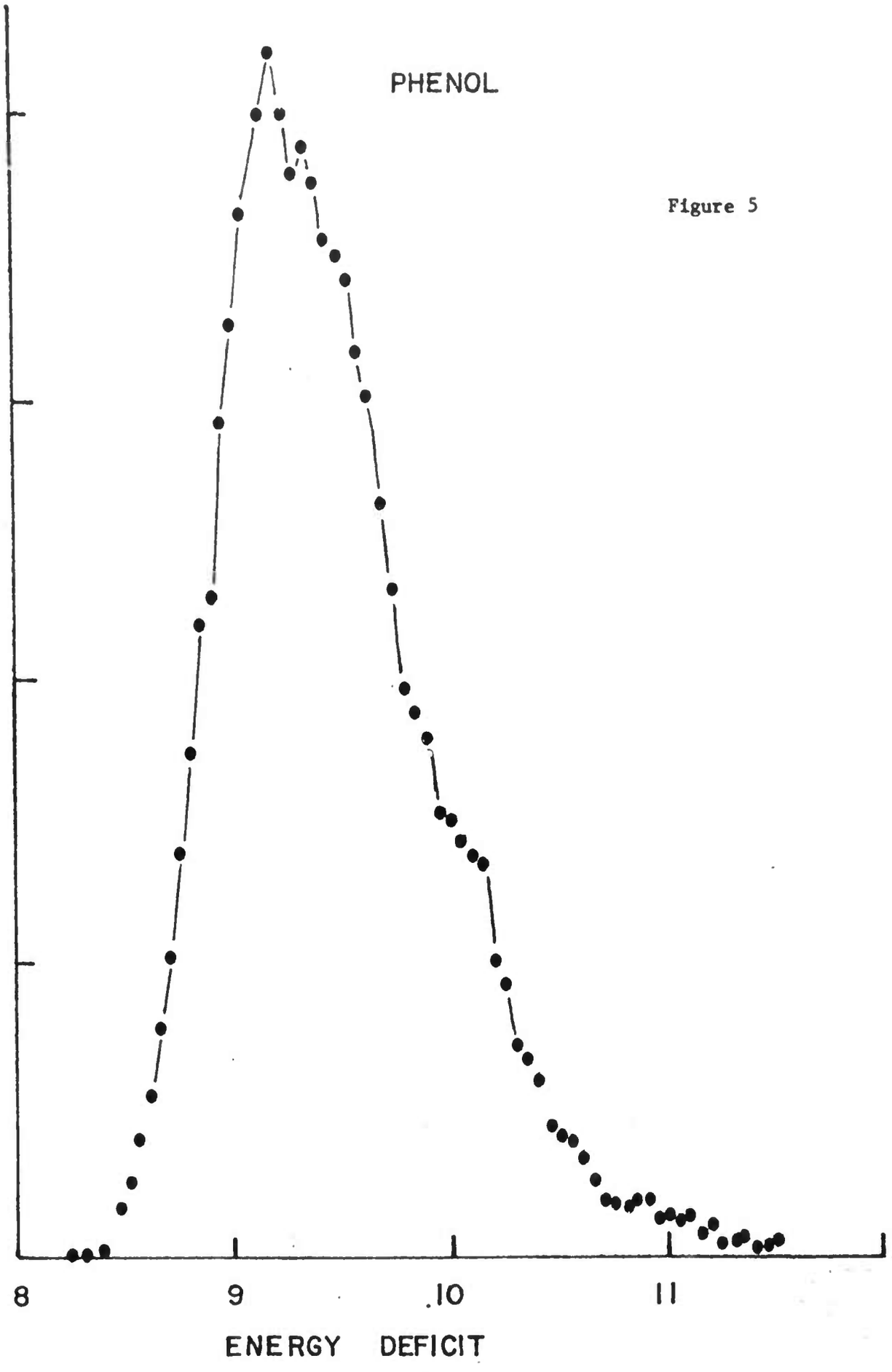

Figure 5